International Journal of Computational Methods
Vol. 15, No. 1 (2018) 1842008 (12 pages)

DOI: 10.1142/S0219876218420082

A Machine Learning-Based Method for Intracoronary Oct Segmentation and Vulnerable Coronary Plaque Cap Thickness Quantification

Xiaoya Guo*, Dalin Tang*,†,‡‡, David Molony‡, Chun Yang†, Habib Samady‡, Jie Zheng§, Gary S. Mintz¶, Akiko Maehara¶, Liang Wang†, Xuan Pei‖, Zhi-Yong Li‖, Genshan Ma**,§§ and Don P. Giddens‡,††

*Department of Mathematics, Southeast University
Nanjing 210096, P. R. China

†Mathematical Sciences Department, Worcester Polytechnic Institute
Worcester, MA 01609, USA

‡Department of Medicine, Emory University School of Medicine
Atlanta, GA 30307, USA

§Mallinckrodt Institute of Radiology, Washington University
St. Louis, MO 63110, USA

¶The Cardiovascular Research Foundation, Columbia University
New York, NY 10022, USA

‖School of Biological Science & Medical Engineering
Southeast University, Nanjing 210096, P. R. China

**Department of Cardiology, Zhongda Hospital
Southeast University Nanjing 210009, P. R. China

††The Wallace H. Coulter Department of Biomedical Engineering
Georgia Institute of Technology, Atlanta, GA 30332, USA
‡‡dtang@wpi.edu
§§magenshan@hotmail.com

Received 4 September 2017
Revised 5 December 2017
Accepted 10 December 2017
Published

Accurate cap thickness quantification is of fundamental importance for vulnerable plaque detection in cardiovascular research. A segmentation method for intracoronary optical coherence tomography (OCT) image based on least squares support vector machine (LS-SVM) was performed to characterize plaque component borders and quantify fibrous cap thickness. Manual segmentation of OCT images were performed by experts based on combination of virtual-histology intravascular ultrasound (VH-IVUS) and OCT images and used as gold standard. The segmentation methods based on LS-SVM provided accurate

‡‡Corresponding author.

plaque cap thickness (an 8.6% error by LS-SVM vs. 71% error by IVUS50) serving as solid basis for plaque modeling and assessment.

Keywords: Vulnerable plaque; coronary; OCT; cap thickness; LS-SVM; segmentation.

1. Introduction

Coronary atherosclerotic plaques often rupture without warning and cause acute syndromes. It is commonly believed that plaque rupture is closely associated with thin fibrous cap which covers a large lipid-rich necrotic core [Tang *et al.* (2014); Virmani *et al.* (2000); Finn *et al.* (2010)]. Intravascular ultrasound (IVUS) has been used to quantify plaque morphology to characterize plaque components. Virtual histology IVUS (VH-IVUS) segments grayscale IVUS data into four tissue types: fibrotic, fibro-fatty, lipid-rich necrotic core (lipid in short) and dense calcified tissue [Kubo *et al.* (2010)]. Although VH-IVUS can provide novel insights into plaque morphology, it has limited resolution of 150–250 microns and is not able to detect thin plaque cap with thickness around 65 μm, the critical threshold value determined from histopathological studies [Virmani *et al.* (2000); Jang *et al.* (2002)]. Better imaging modality is needed for vulnerable plaque detection.

In recent years, optical coherence tomography (OCT) has emerged as an imaging modality to identify vulnerable plaques with enhanced future risk predictions. This medical imaging technology has a resolution of approximately 10 μm which is far better than what IVUS could achieve. Therefore, OCT could characterize plaque morphology with much enhanced accuracy [Tearney *et al.* (2012); Bezerra *et al.* (2009)]. Currently, segmentation of OCT images (determination of lumen and plaque components) is mainly performed by researchers manually [Jang *et al.* (2005); Yabushita *et al.* (2002)]. Raber *et al.* [2012] introduced a manual method combined IVUS/VH-IVUS and OCT images to characterize plaque structure. The Combination of VH-IVUS and OCT would complement each other and provide the whole vessel image from IVUS and accurate cap thickness from OCT [Mintz (2015)]. However, manual segmentation is a time-consuming procedure and it also suffers higher inter- and intra-user variability. To overcome these limitations, some semi-automatic and fully-automatic segmentation approaches have been proposed. A method using attenuation coefficients was developed to characterize plaques [Xu *et al.* (2008); Van Soest *et al.* (2010)]. Wang *et al.* [2010] introduced a semiautomatic segmentation for calcified plaques in signal-poor regions with sharply delineated borders in OCT images. After that, they provided semi-automatic segmentation using a dynamic programming algorithm to quantify fibrous cap [Wang *et al.* (2012)]. Athanasiou *et al.* [2014] developed an automated OCT segmentation method for superficial plaque compositions. Some researchers used support vector machine (SVM) to classify plaque components [Shalev *et al.* (2015); Gargesha *et al.* (2015)]. Most methods in the current literature aimed at segmenting high quality images. However, image quality would be worsened due to artifacts of bifurcation, thrombus, and residual

blood, etc. Accurate detection of lipid is still an area requiring cutting-edge research.

While OCT has high resolution and can quantify thin cap thickness, it has limited penetration (1 mm to 2 mm) and is often unable to provide complete information for the whole vessel, especially at locations with large lumen, bifurcation and increased plaque burden [Tearney *et al.* (2012)]. In this paper, we introduce an OCT segmentation method to characterize the plaque component borders and quantify fibrous cap thickness when image quality is not high enough, including the location of bifurcation. Support vector machine was used in separating lipid component and vessel tissue. Validation was performed based on manual segmentation from experts combining VH-IVUS and OCT images.

2. Data and Methods

2.1. *Data acquisition*

In vivo OCT data were acquired from one patient (male, age 51) using ILUMIEN OPTIS System (St. Jude, Minnesota, MN) with informed consent obtained. The OCT catheter was traversed to the segment of interest. An automatic pullback at 20 mm/s was performed. OCT raw data were logarithmically compressed into grayscale images with pixel intensity recorded in polar coordinates which then was converted to Cartesian coordinates for image processing. OCT images in Cartesian coordinates consists of 1024 by 1024 pixels representing a real physical size of 10 mm by 10 mm (pixel size: 9.9 by 9.9 micron).

IVUS images were recorded for the same segment of coronary (Volcano Therapeutics, Rancho Cordova, CA). Following the OCT image acquisition, the IVUS catheter was traversed distally through the artery to the same segment at an automatic pullback speed of 0.5 mm/s. Colored VH-IVUS images were created with different colors to differentiate four plaque types: fibrous, fibro-fatty, lipid and dense calcified tissue (calcification, Ca in short) (see Fig. 1(a)). The positions of both catheters were recorded with angiography for co-registration of OCT and IVUS images.

Nine OCT image slices were selected from the OCT data set of this patient co-registered VH-IVUS images. Images from the locations of bifurcation were also

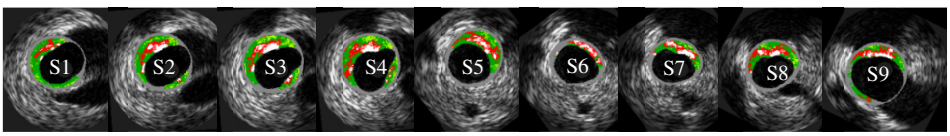

(a) VH-IVUS Slices

Fig. 1. Nine matching VH-IVUS and OCT image slices and manual segmented contours. Colors used in VH-IVUS: *Red* necrotic core, *White* dense calcium, *Dark Green* Fibrous, *Light Green* Fibro-Fatty.

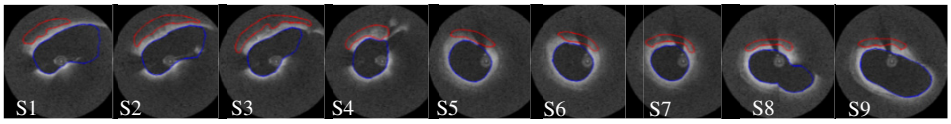

(b) Matching OCT Slices and Manual Segmented Contours

Fig. 1. (*Continued*)

considered. Tiny calcium was neglected in OCT images. Manual lipid contours were obtained from experts based on the combination of VH-IVUS and OCT images following the standard procedure described in Raber *et al.* [2012]. The manual lipid delineation was considered as the standard for classification in least squares support vector machine (LS-SVM) and saved as image masks for comparison with our segmentation. Figure 1 shows VH-IVUS and OCT images as well as segmented overlapping lipid and lumen contours.

2.2. *Image processing*

OCT images in polar coordinates were processed to detect lumen border [Ughi *et al.* (2013)]. Since fibrous cap was the main focus in this study, the lumen border was expanded from center of catheter outward 1 mm as the outer border to include enough space for fibrous cap characterization. At the locations of bifurcation, branches of the coronary without catheter passing through were removed along with its artifacts. Thus the region of interest (ROI) was determined as the area bounded by lumen and outer border with artery branches and other artifacts removed. The ROI of 9 slices are shown in Fig. 2.

2.3. *Feature extraction and selection*

Local binary patterns (LBPs), Gray level co-occurrence matrices (GLCMs), entropy and mean value were calculated as features in this work. All features were computed in an 11 by 11 pixels' neighborhood window in ROI [Athanasiou *et al.* (2014)]. Rotation invariant LBPs with P = 8, R = 1 was used here to extract ten features. Twenty-eight features were selected to improve the accuracy which contains 16 GLCMs (The four contrast, correlation, energy and homogeneity features at each angle $\Theta = 0, 45, 90, 135$ degree), 10 LBPs, entropy and mean value. These 28

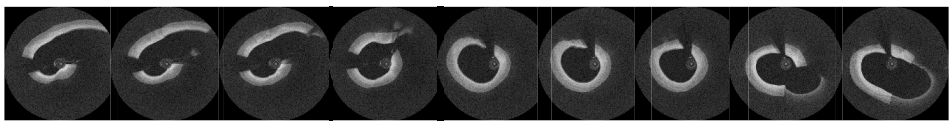

Fig. 2. Nine OCT images with ROI and borders of ROI.

features were the optimal feature combination to reach the highest accuracy for our classification algorithm based on this set of OCT images.

2.4. *Classification*

The database to feed SVM was assembled by all selected features extracted from all pixels in ROI into a data matrix with dimension n by m, where n is equal to the number of pixels and m is 28, the length of the feature vector. Since fibrous cap could be identified once the lipid area is determined, only two classes need to be characterized indicating two different tissue types: lipid and vessel tissue. Fibrous tissue and fibro-fatty tissue have no impact on the measurement of fibrous cap, so they are considered as vessel tissue. LS-SVM follows the structural risk minimization principle of kernel function as learning machine which improves the conventional SVM. LS-SVM classifier was chosen to classify the lipid and vessel tissue with Gaussian Radial Basis Function as the kernel function and steepest descent method for searching optimal parameters [Suykens *et al.* 1999; 2002].

Two methods were proposed to select the training data set to fit SL-SVM classifier. In the first method (denoted as M1), 500 pixels were randomly selected from each lipid class and vessel tissue class for 9 OCT images. The training data set would be the feature vectors from 9000 pixels. The rest of non-selected pixels in ROI of each image would be treated as testing data set. The process was repeated ten times to stabilize the classification error estimation. In the second method (denoted as M2), a procedure similar to leave-one-out cross validation was employed as any 8 out of 9 images were used as training data while the remaining one as the testing data. For each group of 8 OCT images, 500 pixels were random selected from lipid class and vessel tissue class each to give 8000 pixels. The testing set consists of all pixels in ROI of the rest one OCT image. The training and testing was done 9 times in this method. Fig. 3 shows 9 images of classification from LS-SVM after processing using M1 and M2.

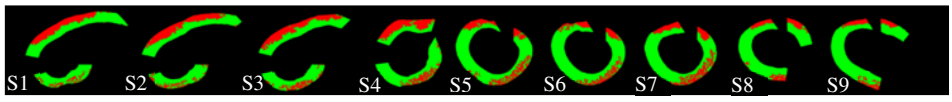

(a) Classification from M1 after processing

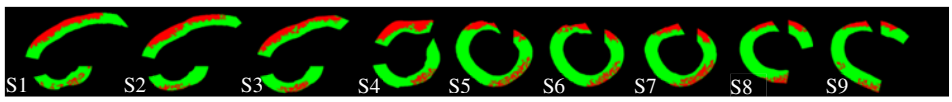

(b) Classification from M2 after processing

Fig. 3. Classification by LS-SVM from M1 and M2. Colors used in Classification images: *Red* necrotic core, *Green* Fibrous and Fibro-Fatty.

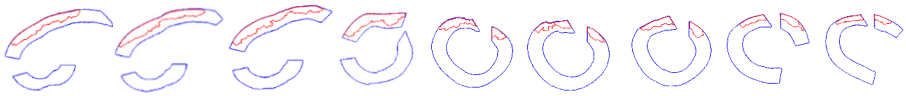

(a) OCT contours from M1

(b) OCT contours from M2

Fig. 4. Lipid contours and borders. Color contours: *Red* lipid contours, *Blue* borders.

2.5. *Contours extraction*

Lipid contours were extracted and its distance with lumen contour were calculated as cap thickness. Plaque cap thickness was the main focus in this study. Therefore, lipid contours were extracted to quantify the cap thickness. According to the classification of LS-SVM, the classification images were processed to extract contours. Some scattered pixels in the images of classification were filtered out to get clear border for fibrous cap. Parametric active contour model was used for the lipid border detection (Fig. 4).

2.6. *Co-registered VH-IVUS segmentation*

Original VH-IVUS data often had lipid core exposed directly to lumen when the physical cap thickness is less than IVUS resolution limit (150–200 micron), i.e., there is no fibrous cap covering the lipid core in VH-IVUS image. A minimum cap thickness has to be set when segmenting VH-IVUS data so that there is fibrous cap covering the lipid cores. In our previous publications, 50 μm and 180 μm cap thickness thresholds were used in VH-IVUS segmentation where 50 μm was chosen as it is a reasonable approximation to thin cap number < 65 μm with a 25 micron

(a) IVUS50 contours

(b) IVUS180 contours

Fig. 5. Segmented contours from IVUS50 and IVUS180. Color contours: *Red* lipid contours, *Blue* borders.

step size. VH-IVUS images were segmented by our custom-made software to obtain the segmented contours denoted as IVUS50 and IVUS180 (see Fig. 5).

3. Results

3.1. *LS-SVM classification accuracy*

The LS-SVM segmentation results were compared to manual segmentation to evaluate the classification accuracy (denoted as Acc) defined as in the following formula:

$$\text{Acc} = \frac{TP + TN}{TP + FP + TN + FN}, \tag{1}$$

where we set lipid and vessel tissue as positive and negative pattern, respectively, TP is the number of true positive outcomes, FP is the number of false positive outcomes, TN is the number of true negative outcomes and FN is the number of false negative outcomes. Sensitivity (Sen) and specificity (Spe) were also calculated using the formulas below to avoid the reliance of the uneven distributed data in two classes.

$$\text{Sen} = \frac{TP}{TP + FN}, \tag{2}$$

$$\text{Spe} = \frac{TN}{TP + FP}. \tag{3}$$

Figure 6 gives the sensitivity and specificity of classification from ten times repeated experiment using M1. Sensitivity was about 10% higher than specificity for most OCT images. For the extreme worst case, specificity would still about 70%, while sensitivity would achieve up to 97% for good cases during the ten times of trial. The average values of sensitivity and specificity were 89.6% and 78.6%, respectively.

Table 1 compares the classification accuracy of M1 and M2. Based on the average values of 9 OCT images, M1 showed a slightly better overall classification accuracy than M2 (M1 (79.7%) vs M2 (76.1%)). For Sensitivity, M1 provided much higher

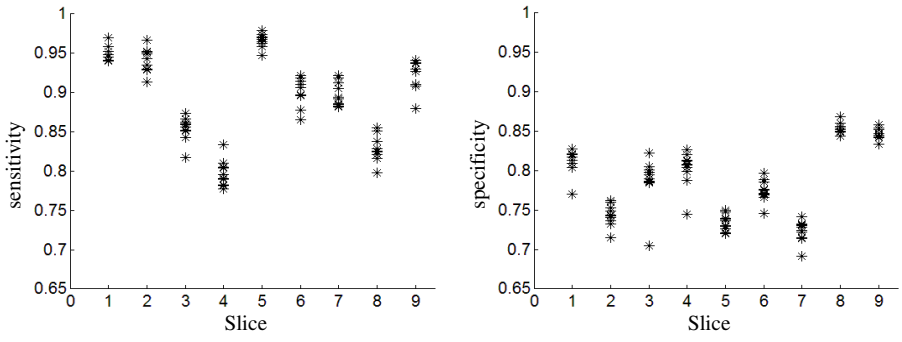

(a) (b)

Fig. 6. Sensitivity and specificity from 10 tests of 9 slices based on Method 1.

Table 1. Segmentation accuracy for lipid and fibrous tissue using M1 and M2.

	M1			M2		
Slice	Sen	Spe	Acc	Sen	Spe	Acc
1	0.950	0.811	0.834	0.829	0.789	0.795
2	0.941	0.743	0.771	0.792	0.714	0.725
3	0.854	0.787	0.799	0.720	0.761	0.754
4	0.797	0.802	0.800	0.648	0.785	0.743
5	0.966	0.734	0.743	0.900	0.685	0.693
6	0.901	0.774	0.782	0.701	0.762	0.758
7	0.898	0.723	0.740	0.787	0.717	0.724
8	0.831	0.855	0.852	0.646	0.844	0.820
9	0.925	0.847	0.854	0.817	0.835	0.834
Ave.	0.896	0.786	0.797	0.760	0.766	0.761

value than M2 (M1 (89.6%) vs M2 (76.0%)) while the specificity values are quite close (M1 (78.6%) vs M2 (76.6%)). The good agreement demonstrated the stability of two automatic segmentation methods proposed.

3.2. *Model comparisons showing OCT provided more accurate cap thickness*

For all 9 co-registered OCT/VH-IVUS images, five different segmentation methods (manual segmentation (denoted as Ma), M1, M2, IVUS50 and IVUS180) were applied to detect the lipid contours and lumen borders. Cap thickness was calculated for regions (identified as cap) between lipid core and lumen. The average value and minimum over the cap were recorded in Table 2 as mean cap thickness and min cap thickness. Using manual segmentation as the gold standard and baseline value, M1 and M2 generally gave better results than IVUS50 and IVUS180. The average of mean cap thickness (9 slices, unit: mm) from 5 methods were 0.561, 0.470, 0.463, 0.128, and 0.204, respectively. Average values from M1 and M2 were approximately the same. The average cap thickness values of M1, M2, IVUS50 and IVUS180 were 16.3%, 17.4%, 77.2% and 63.6% less than Ma, respectively. Average of minimum cap thickness (9 slices) from 5 methods were 0.390, 0.288, 0.282, 0.040, and 0.165, respectively. The average min values of M1, M2, IVUS50 and IVUS180 were 26.0%, 27.5%, 89.6% and 57.6% less than Ma, respectively.

3.3. *Point-to-Point cap thickness comparison*

Cap thickness data from the five segmentation methods were compared by point-to-point method to obtain more precise assessment of the methods. The min cap thickness of 9 slices ranged from 0.158 mm to 0.497 mm. The matching points of Slice 1 and Slice 4 from five methods are showed in Fig. 7. Figure 8 shows the scatter diagram of Slice 1 and Slice 4 which gave the cap thickness of matched points from five methods. Point 1-Point 4 based on Ma from slice 4 were close to

Table 2. Mean cap thickness and minimum cap thickness for 9 slices from five methods.

	Mean Cap Thickness (mm)								
Slice	Ma	M1	Error	M2	Error	IVUS50	Error	IVUS180	Error
1	0.957	0.484	18.9%	0.459	23.1%	0.166	72.2%	0.239	60.1%
2	0.683	0.483	29.2%	0.446	34.8%	0.123	82%	0.208	69.5%
3	0.765	0.492	35.7%	0.478	37.5%	0.094	87.8%	0.196	74.4%
4	0.337	0.383	13.5%	0.350	3.9%	0.120	64.5%	0.203	39.8%
5	0.575	0.399	30.6%	0.455	20.9%	0.173	69.9%	0.216	62.5%
6	0.491	0.484	1.3%	0.459	6.5%	0.087	82.3%	0.178	63.6%
7	0.477	0.412	13.6%	0.412	13.7%	0.139	70.9%	0.209	56.2%
8	0.539	0.572	6.2%	0.549	1.9%	0.144	73.3%	0.210	61.1%
9	0.584	0.515	11.9%	0.561	4.7%	0.103	82.3%	0.181	69%
Ave.	0.561	0.470	16.3%	0.463	17.4%	0.128	77.2%	0.204	63.6%
	Min Cap Thickness (mm)								
1	0.497	0.308	38%	0.314	36.9%	0.050	89.8%	0.172	65.4%
2	0.429	0.330	23.1%	0.225	47.6%	0.042	90.2%	0.165	61.5%
3	0.539	0.285	47.2%	0.285	47.2%	0.035	93.5%	0.170	68.5%
4	0.158	0.150	5.0%	0.163	3.0%	0.033	78.9%	0.159	0.5%
5	0.331	0.163	50.8%	0.227	31.6%	0.042	87.4%	0.165	50.3%
6	0.326	0.285	12.7%	0.274	16.0%	0.039	88.1%	0.162	50.5%
7	0.392	0.338	13.7%	0.295	24.7%	0.043	89.2%	0.167	57.3%
8	0.445	0.413	7.3%	0.427	4.0%	0.050	88.7%	0.164	63.1%
9	0.390	0.324	16.8%	0.333	14.5%	0.030	92.4%	0.163	58.2%
Ave.	0.390	0.288	26.0%	0.282	27.5%	0.040	89.6%	0.165	57.6%

180 μm (see Fig. 8(b)). By using Ma values as baseline (100%), the differences of cap thickness were 9.7% (M1) and 8.6% (M2). The cap thickness values from IVUS180 were overestimated about 8.2% than the value from Ma. The cap thickness values from IVUS50 were underestimated about 71.0% than the cap thickness from Ma.

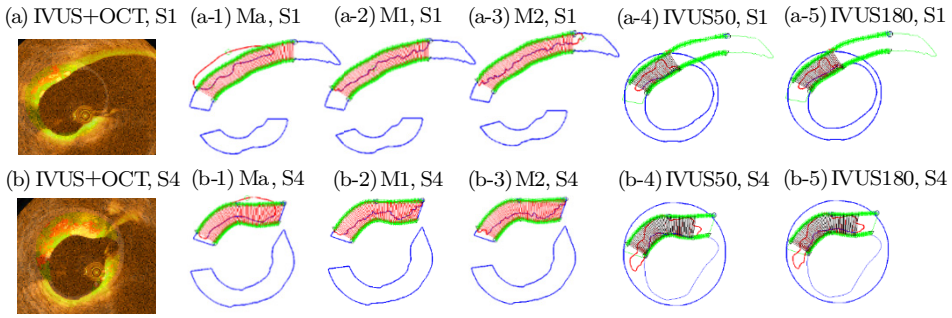

Fig. 7. The point-point cap thickness in Slice 1 and Slice 4. (a) S1 OCT image overlaid with S1 IVUS image. (b) S4 OCT image overlaid with S4 IVUS image. (a-1) cap thickness from Manual segmentation in Slice 1. (a-2) cap thickness from M1 in Slice 1. (a-3) cap thickness from M2 in Slice 1. (a-4) cap thickness from IVUS50 in Slice 1. (a-5) cap thickness from IVUS180 in Slice 1. (b-*) is similar to (a-*), but it is for Slice 4.

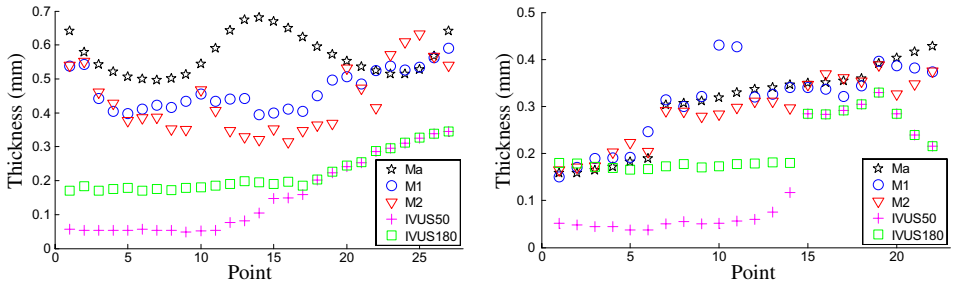

(a) Point-point cap thickness in S1 (b) Point-point cap thickness in S4.

Fig. 8. Scatter diagram of point-point cap thickness from slice 1 and slice 4 using 5 methods.

Point 10–14 based on Ma from slice 4 were about 300 μm. The differences of cap thickness were 15.1% (M1) and 10.3% (M2) compared with Ma. The cap thickness of IVUS50 and IVUS180 were underestimated by about 78.5% and 46.7%. Point 5–8 and point 20–26 based on Ma from slice 1 were close to 500 μm (see Fig. 8(a)). The differences of cap thickness were 12.2% (M1) and 23.3% (M2) compared with Ma. The cap thickness of IVUS50 and IVUS180 were underestimated by about 84.0% and 71.9%. The cap thickness values of two segmentation methods (IVUS50 and IVUS180) were largely determined by the previously educated guesses.

4. Discussion

4.1. *Signification of OCT images for cap thickness*

Imaging resolution has been a major limitation for vulnerable plaque research (and other areas in a broader sense) since the introduction of medical imaging. With image resolutions at 150 μm (IVUS)–300 μm (MRI) or even worse, and plaque vessel wall thickness changes were normally under 200 μm, and "vulnerable plaque" cap thickness threshold value defined as 65 μm, many published results were educated guesses by segmentation software. With the capability of detecting thin fibrous cap, OCT is able to provide more accurate cap thickness information to enhance both the morphological and mechanical analyses in vulnerable plaque research.

4.2. *Prediction for cap thickness*

Using manual segmentation as standard, it was shown that IVUS50 and IVUS180 underestimated the real cap thickness for the sample studied. In particular, IVUS50 demonstrated worse accuracy in estimating the cap thickness. Regarding to some particular thickness values, IVUS180 provided relatively accurate cap thickness measurement when the cap thickness is about 180 μm. It should be noted that IVUS accuracy depends on real plaque cap thickness. For thin cap plaques, IVUS50 may have better accuracy that IVUS180. In any case, the segmentation with combination of IVUS and OCT images provided more accurate cap thickness.

Among the different segmentation methods, predictions from LS-SVM (M1 and M2) showed higher agreements with manual segmentation in measuring mean cap thickness, comparing to IVUS50 and IVUS180. The relative error between M1/M2 and manual segmentation is less than 17.4% for mean cap thickness, and less than 27.5%, if we look at the minimum cap thickness. More accurate prediction for cap thickness will provide the important foundation for mechanical analysis of coronary atherosclerosis.

4.3. *Limitations*

One major limitation of this study is lack of histology data as the golden standard. Manual segmentation results based on IVUS and OCT images were considered as the alternative to the golden standard. Another limitation is the small sample size of OCT image studied. Large-scale studies with more OCT image are needed to validate and improve the significance of prediction method.

5. Conclusion

A segmentation method for OCT images based on LS-SVM using manual segmentation combined with VH-IVUS data as gold standard was introduced for more accurate plaque cap thickness quantification. The segmentation method combining OCT and IVUS images showed considerable improvement for cap thickness quantification over the segmentation method using only IVUS images.

Acknowledgments

This research was supported in part by NIH grant R01 EB004759 and a Jiangsu Province Science and Technology Agency grant BE2016785.

References

Athanasiou, L. S. *et al.* [2014] "Methodology for fully automated segmentation and plaque characterization in intracoronary optical coherence tomography images," *J. Biomed. Opt.* **19**, 026009–026009.

Bezerra, H. G. *et al.* [2009] "Intracoronary optical coherence tomography: A comprehensive review: Clinical and research applications," *JACC-Cardiovasc. Interv.* **2**, 1035–1046.

Finn, A.V. *et al.* [2010] "Concept of vulnerable/unstable plaque," *Arterioscler. Thromb. Vasc. Boil.* **30**(7), 1282–1292.

Gargesha, M. *et al.* [2015] "Parameter estimation of atherosclerotic tissue optical properties from three-dimensional intravascular optical coherence tomography," *J. Med. Imaging* **2**, 016001–016001.

Jang, I. K. *et al.* [2002] "Visualization of coronary atherosclerotic plaques in patients using optical coherence tomography: Comparison with intravascular ultrasound," *J. Am. Coll. Cardiol.* **39**, 604–609.

Jang, I. K. *et al.* [2005] "In vivo characterization of coronary atherosclerotic plaque by use of optical coherence tomography," *Circulation* **111**, 1551–1555.

Kubo, T. *et al.* [2010] "The dynamic nature of coronary artery lesion morphology assessed by serial virtual histology intravascular ultrasound tissue characterization," *J. Am. Coll. Cardiol.* **55**, 1590–1597.

Mintz, G. S. [2015] "Optical Coherence Tomography and Virtual-Histology Intravascular Ultrasound Strange Bedfellows? or Not?," *Circ. Cardiovasc. Imaging* **8**, e004045.

Räber, L. *et al.* [2012] "Offline fusion of co-registered intravascular ultrasound and frequency domain optical coherence tomography images for the analysis of human atherosclerotic plaques," *EuroIntervention* **8**, 98–108.

Shalev, R. *et al.* [2015] "Intravascular optical coherence tomography image analysis method," *Biomedical Engineering Conf.* (*NEBEC*), 41st Annual Northeast. IEEE, pp. 1–2.

Suykens, J. A. K. and Vandewalle, J. [1999] "Least squares support vector machine classifiers," *Neural Process. Lett.* **9**, 293–300.

Suykens, J. A. K., Van Gestel, T. and De Brabanter, J. [2002] *Least Squares Support Vector Machines.* World Scientific.

Tang, D. *et al.* [2014] "Image-based modeling for better understanding and assessment of atherosclerotic plaque progression and vulnerability: data, modeling, validation, uncertainty and predictions," *J. Biomech.* **47**(4), 834–846.

Tearney, G. J. *et al.* [2012] "Consensus standards for acquisition, measurement, and reporting of intravascular optical coherence tomography studies," *J. Am. Coll. Cardiol.* **59**, 1058–1072.

Ughi, G. J. *et al.* [2013] "Automated tissue characterization of in vivo atherosclerotic plaques by intravascular optical coherence tomography images," *Biomed. Opt. Express* **4**, 1014–1030.

Van Soest, G. *et al.* (2010) "Atherosclerotic tissue characterization in vivo by optical coherence tomography attenuation imaging," *J. Biomed. Opt.* **15**, 011105.

Virmani, R. *et al.* (2000) "Lessons from sudden coronary death: A comprehensive morphological classification scheme for atherosclerotic lesions," *Arterioscler. Thromb. Vasc. Biol.* **20**, 1262–1275.

Wang, Z. *et al.* [2010] "Semiautomatic segmentation and quantification of calcified plaques in intracoronary optical coherence tomography images," *J. Biomed. Opt.* **15**, 061711.

Wang, Z. *et al.* [2012] "Volumetric quantification of fibrous caps using intravascular optical coherence tomography," *Biomed. Opt. Express* **3**, 1413–1426.

Xu, C. *et al.* [2008] "Characterization of atherosclerosis plaques by measuring both backscattering and attenuation coefficients in optical coherence tomography," *J. Biomed. Opt.* **13**, 034003-8.

Yabushita, H. *et al.* [2002] "Characterization of human atherosclerosis by optical coherence tomography," *Circulation* **106**, 1640–1645.